NOTA TÉCNICA

AEMCC

Northern hemisphere wintertime teleconnections: impact of time-averaging

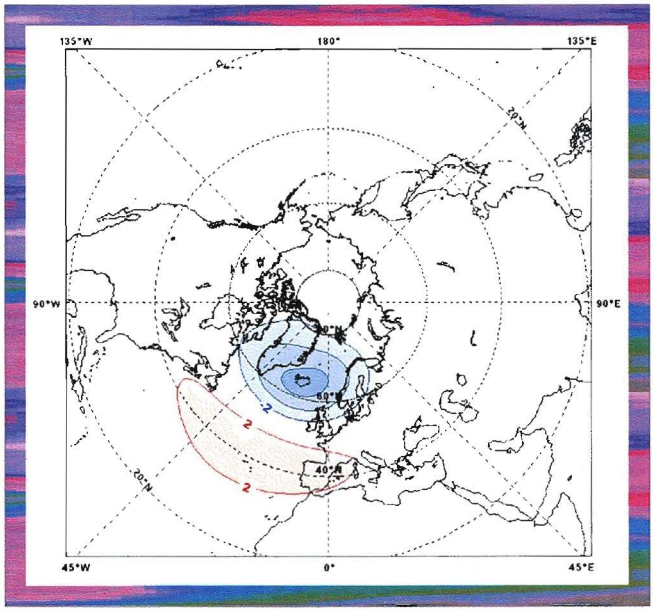

Nota Técnica AEMCC N.º 1

MINISTERIO DE MEDIO AMBIENTE

DIRECCIÓN GENERAL DEL INSTITUTO NACIONAL DE METEOROLOGÍA

NT

EMCC 1

Northern hemisphere wintertime teleconnections: impact of time-averaging

Nota Técnica 1

Área de Evaluación y Modelización del Cambio Climático
Subdirección General de Climatología y Aplicaciones
Instituto Nacional de Meteorología

María Jesús Casado Calle [1]
Francisco Javier Doblas-Reyes [2]
María Asunción Pastor Saavedra [1]

[1] Instituto Nacional de Meteorología (INM)
Calle Leonardo Prieto Castro, 8, 28071, Madrid, Spain

[2] European Centre for Medium-Range Weather Forecasts (ECMWF)
Shinfield Park, RG2 9AX, Reading, United Kingdom

MINISTERIO DE MEDIO AMBIENTE
INSTITUTO NACIONAL DE METEOROLOGÍA

2006

Nota Técnica 1 del Área de Evaluación y Modelización del Cambio Climático (NT AEMCC-1)
Instituto Nacional de Meteorología

Edita: Centro de Publicaciones
Secretaría General Técnica
Ministerio de Medio Ambiente ©

ISBN: 84-8320-360-X
NIPO: 310-06-102-0
Depósito Legal: M-39677-2006
Imprime: Imprenta del Instituto Nacional de Meteorología

TABLE OF CONTENTS

Pág.

1. Introduction 4
2. Data 5
3. Diagnostics techniques 6
4. Characteristics of the teleconnection patterns 7
5. Summary and concluding remarks 12
6. Acknowledgements 12
7. Bibliography 13
8. List of tables 15
9. Figures 17

1. Introduction

Understanding the sources of low-frequency intraseasonal variability has long been one of the major targets in climate studies. The extratropical intra-seasonal variability has in some cases been characterized in terms of space-stationary and time fluctuating structures known as "teleconnection patterns" (Wallace and Guztler, 1981; Barnston and Livezey, 1987; Monahan, 2000). These atmospheric patterns have had a large impact on the understanding of the variability on interannual and longer timescales, because they play an important role in the global climate system (Thompson and Wallace, 2001; Franzke et al., 2004). The processes involved in the evolution of several of the teleconnections are not fully identified, being of key importance to improve the predictive ability at several time scales (Branstator, 2002).

As pointed out by Panagiotopoulos et al. (2002), despite the advantages of having detailed knowledge of the structure of the teleconnection patterns, progress in this topic has been relatively slow and unsatisfactory compared to other aspects of the meteorological science. One of the main reasons is the lack of universally accepted criteria and procedures for defining teleconnection patterns. In this sense, Quadrelli and Wallace (2004) suggested that the different analysis techniques used for their detection also yield different patterns, and even the same technique can yield quite different results depending on the dataset used. The patterns that have emerged in previous studies have been conditioned by the spatial domain of the analysis, the manner in which seasonality is treated, and the time interval over which the data are averaged before the analysis is performed. This uncertainty could be reduced with a systematic intercomparison of the pattern properties obtained in a common framework.

One of these aspects, namely the effect of different temporal averaging timescales on the regime structure of the Northern Hemisphere extratropical atmosphere has been studied by Teng et al. (2004) in the context of climate regimes. That work

emphasises the sensitivity of regime properties to the time filtering of the data demonstrating the need to carefully consider the averaging time scale. This is in agreement with FELDSTEIN (2000), who mentioned that although there are valuable benefits to using time averaged data, especially from the perspective of long-range forecasting, such time averaging could obscure some of the short scale properties underlying the dynamical processes.

The work described here has been mainly motivated by the debate involving the convenience of the use of monthly or seasonal averaged data instead of daily data. In order to determine whether there is any sensitivity, we look at the spatio-temporal features of the leading teleconnection patterns obtained by rotated empirical orthogonal functions (REOFs) technique when different time averaging is applied.

In section 2, we describe the data used. This is followed in section 3 by a description of the diagnostic techniques. In section 4, we describe the most relevant results of the possible effects of time averaging in the spatial and temporal characteristics of the teleconnections, and finally the summary and concluding remarks are given in section 5.

2. DATA

Gridded daily (12 UTC) 500-hPa geopotential height data from two quasi-independent reanalysis datasets over the period 1957-2002 have been used: the European Centre for Medium-Range Weather Forecast dataset (ERA-40 henceforth, UPPALA ET AL., 2005) and the National Centers for Environmental Prediction dataset (NCEP henceforth, KALNAY ET AL., 1996). Daily anomalies are computed by removing the mean seasonal cycle at each grid point. The mean seasonal cycle is estimated as the sum of the annual average and the first four Fourier harmonics of the daily climatology. The analysis has been carried out for the extended winter season December-to-March, (DJFM henceforth). This season has been selected since the boreal

winter shows the largest variability over the extratropical latitudes (e.g. Kushnir and Wallace, 1989; Blackmon et al., 1984). The spatial domain extends north of 20ºN.

From the original daily data (C1 henceforth), two additional datasets are generated with a different time sampling. A 10-day low pass filtered dataset (C2 henceforth) is created by applying a digital low-pass filter (Bloomfield, 1976; Doblas-Reyes and Déqué, 1998). The third dataset consists of monthly means (C3 henceforth). The standard deviation maps for the three datasets (daily, 10-day low-pass filtered and monthly) are shown in Figure 1. Every map exhibits two maxima located over the Pacific and Atlantic. A reduction of the variance is found in the filtered and monthly mean data.

3. Diagnostic techniques

An empirical orthogonal function (EOF) analysis based upon the covariance matrix has been applied to the anomalies of each of the three datasets (C1, C2 and C3). Prior to the eigenvector analysis, the anomalies were weighted with the square root of the normalised cosine of the latitude.

A shortcoming of EOF analysis is that eigenvectors are mathematical constructions, constrained by their mutual orthogonality and the maximization of variance over the entire analysis domain. The use of EOFs can predispose the analysis to merging or blending patterns of variability that would be otherwise independent (Richman, 1986). An alternative to reduce the effect of this drawback consists in rotating the empirical orthogonal functions and the corresponding orthonormal principal component time series (PC). This way, the areas where the maxima of variability occur tend to be more concentrated. A criticism of rotated EOFs (REOFs) (Hannachi, 2004) is the potential arbitrariness of the results due to the subjective choice of the following: *a)* the number of modes to rotate and *b)* the type of rotation scheme used, which could be either orthogonal or oblique. As pointed out by Hannachi (2004),

the debate over when and how to rotate EOFs and PCs continues to generate, at times, important discussions. In this study, we have rotated the 14 leading EOFs using a varimax orthogonal rotation. The EOFs have been previously renormalized following the rule suggested by VON STORCH AND ZWIERS (1999), where the renormalized EOFs carry the units of the field and the PCs have unit variance. The fraction of total variance for ERA-40 explained by the retained EOFs is 63%, 75% and 85% for the C1, C2 and C3 datasets, respectively. The fraction of variance on the NCEP data shows identical results. Note the increase with the filtering in the percentage of variance.

4. CHARACTERISTICS OF THE TELECONNECTION PATTERNS

The set of wintertime northern extratropics teleconnection patterns commonly identified in the literature (WALLACE AND GUTZLER, 1981; BARNSTON AND LIVEZEY, 1987; BELL AND HALPERT, 1995) has been found in the datasets studied here. The main patterns identified are: North Atlantic Oscillation (NAO), Pacific North American (PNA), West Pacific (WP), Scandinavian (SCA), East Atlantic/Western Russia (EA/WR), East Atlantic (EA), and East Pacific (EP). For the sake of simplicity, the following description focuses on NAO, SCA, PNA and WP.

Table 1 shows the fraction of total variance explained by the teleconnection patterns obtained with the ERA-40 reanalyses. The NCEP reanalysis provides similar results, except for a decrease of the NAO variance when using monthly means. The small differences between ERA-40 and NCEP could be used as an estimate of the uncertainty in the estimated properties of the teleconnection patterns. The variance fraction increases from daily to a maximum with the monthly mean data. While the fraction of variance is very similar among all teleconnection patterns when using daily and filtered data, the NAO and PNA stand out as the leading patterns when monthly data are used. FELDSTEIN (2000) found a similar result working with daily 300 hPa height data and rotating the leading eight EOFs. This suggests that data averaging allows to discriminate be-

tween two types of patterns, with larger scale patterns such as the NAO and PNA explaining more variance than wave-like patterns when longer time scales (from daily to monthly) are considered.

Though the usual procedure involves the use of monthly or seasonal data, only more recently, several authors have pointed out the convenience of working with daily data to capture full detail of the characteristics of these patterns. Daily data allow the computation of a typical time scale of the teleconnection. Following FELDSTEIN (2000), an e-folding time can be defined for the Rotated Principal Component (RPC) time series as the time taken for the autocorrelation function of each RPC time series to decrease by a factor of e. The teleconnection e-folding times are 7.9, 13.0, 7.8 and 11.6 days, with a good agreement between both reanalyses. These time scales are quite similar to those found by METZ (1991) for the PNA/WP and NAO/EA patterns (9 and 8 days, respectively) and also similar to those found by FELDSTEIN (2000). The e-folding times are higher than the time scales associated with synoptic scale waves (~4 days) and, more importantly, suggest that the teleconnection patterns have an important intra-monthly component that is not taken into account when using monthly mean data.

The NAO (Fig. 2) pattern differs from the reference pattern from the Climate Prediction Center (CPC) in an eastwards displacement of the northern part of the dipole. There are some differences among the three datasets in the northern part of the dipole, which is located over central Iceland in C3 and eastern Iceland for C1 and C2. The SCA pattern (not shown) differs from that of the CPC in an eastern displacement of the Scandinavian centre and the absence of the secondary western European centre in C1 and C2 datasets. A strong similarity in the location of centres over Scandinavia and Mongolia can be found between the three datasets. The PNA pattern (Fig. 3) differs from the CPC pattern in the centre located over south-eastern North America, which is absent in all three datasets. Furthermore, the northwestern North American centre is shifted

slightly westwards in C1 and C2. As Rodionov and Assel (2001) mentioned, distorted PNA patterns are often revealed in Principal Component Analysis of the 700-hPa and 500-hPa height fields, with the centers of action shifted 10º-15º from the classical PNA pattern described by Wallace and Gutzler (1981). The WP pattern (not shown) differs from the reference in the smaller extension of the southern part of dipole, mainly in C1 and C2.

The spatial correlation coefficient between the different patterns has been used as a measure of similarity. Table 2 shows very high correlations for the ERA-40 reanalysis (similar results are found for NCEP). The highest correlations are detected between daily unfiltered data (C1) and 10-day low-pass filtered data (C2). These results suggest that the spatial patterns are a robust feature of the teleconnections. The similarity in the time series associated with each teleconnection pattern has been measured using time correlations. As in the case of the spatial patterns, the time series are highly correlated (~0.9) and statistically significant. Therefore, to a large extent the teleconnection patterns computed using monthly mean data should give similar results to the patterns computed with daily or low-pass filtered data. The overall agreement in the analysis carried out on both reanalysis supports this.

However, other characteristics of the teleconnection time series are the deviations from gaussianity. These deviations can be measured using the skewness b_1 and kurtosis (b_2 - 3), where $b_1 = m_3/m_2^{3/2}$ and $b_2 = m_4/m_2^2$, m_k being the kth moment about the mean. The skewness measures the asymmetry of the probability distribution about the mean, while the kurtosis measures its flatness (Jolliffe and Stephenson, 2003). The skewness coefficients of the ERA-40 teleconnection patterns are shown in Table 3. The coefficients in bold are significant with a 95% confidence, where the standard $\sqrt{b_1}$ test (García Pérez, 1992) has been used. The C1 and C2 datasets (daily data) correspond to asymmetric distributions (skewness different from zero), while only the WP pattern shows the same

behaviour in the case of monthly data. In the C1 and C2 cases, skewness is positive for SCA, indicating that extreme values tend to be more positive than negative. On the contrary, NAO, PNA and WP are left-skewed distributions, indicating a large tail to the negative values. While there is a strong agreement between both reanalyses for the results with daily data, the C3 dataset shows large differences in skewness between ERA-40 and NCEP for NAO.

Kurtosis measures the relative frequency of rare events with respect to the standard deviation (JOLLIFFE AND STEPHENSON, 2003). Positive (negative) kurtosis indicates a relatively peaked distribution with long (short) tails or leptokurtic (platykurtic). Table 4 shows the b_2 - 3 kurtosis coefficients for ERA-40. The coefficients in bold represent the values significantly different from zero with a 95% confidence following the standard b_2 test (GARCÍA PÉREZ, 1992). NAO, SCA and PNA show negative kurtosis in C1 and C2 (statistically significant in the first two). This platykurtic behavior indicates that the tails of the respective distributions present a low probability and that extreme events are relatively rare. WP depicts a positive kurtosis in the case of daily data, although not significant in the C2 case. The C3 dataset displays no significant values with any of the two reanalyses used.

The skewness and kurtosis of the C1, C2 and C3 datasets suggest that the teleconnection time series obtained with monthly means are more Gaussian due to the central limit theorem. This has important consequences when the teleconnection patterns are used in the study of extreme events, as the use of monthly means will mask the occurrence of the patterns with the largest amplitude, which given the e-folding time scale of the patterns should happen in a time scale of a few days.

These results above suggest that the shape of the probability distribution function (PDF) of the teleconnection time series differs between the patterns, as some are left skewed and leptokurtic (WP) while others are right skewed and platykurtic

(SCA). Interestingly, the two larger-scale patterns, NAO and PNA, are both left skewed and platykurtic. Figure 4 shows the PDFs of the four patterns. The PDFs were estimated using a Gaussian kernel estimator (SILVERMAN, 1986) with a smoothing parameter equal to 0.40. A simple look does not detect large differences between the C1 and C2 PDFs. However, the PDFs obtained with monthly data are more irregular due to the smaller sample used. This is more obvious in the case of the WP pattern. This could explain the larger differences obtained in the parameters of the C3 dataset.

Three non-parametric statistics have been estimated to summarize the characteristics of the probability distributions: the median (MED), the interquantile-range (IQR) and the Yule-Kendall (YKI) skewness (WILKS, 1995). These are robust measures of the location, scale (or spread) and shape (or skewness) because they are insensitive to the tail ends of the PDF. The YKI is computed by comparing the distance between the median and each of the two quartiles and the IQR refers simply to the difference between the upper and lower quartiles. Table 5a shows the estimates for ERA-40. There is a change of sign of both the estimates of the median and the YKI between C1/C2 and C3 for the NAO that indicate a clear change in skewness. Although this behaviour is not clearly evidenced in Table 3, HANNACHI ET AL. (2003) point out that parametric skewness is a non-robust estimator and might be sensitive to outliers. The WP PDF is the more peaked distribution in C2 and C3 data, especially in C3, this result corroborates the results obtained in the analysis of kurtosis when parametric measures have been employed. There is a strong agreement between the statistics obtained with the ERA-40 and NCEP (Table 5b) reanalyses.

In spite of the agreement between the spatial patterns, the finer detail in the PDF of the teleconnection time series supports the need of considering their computation using daily or low-pass filtered data, especially if the patterns are to be used in the analysis of extreme events.

5. Summary and concluding remarks

Some of the well-known 500-hPa wintertime teleconnection patterns are examined here in a preliminary way to determine whether or not any significant difference, spatial or temporal can be found when different time averaging is applied in two reanalyses. The evidence suggests that some differences exist.

The spatial structures are rather insensitive to the time averaging. This behaviour may point to the fact that the atmospheric variability, as long as its spatial structure is concerned, is not so dependent on time averaging in spite of the relatively low life timescales. These results are in agreement with those of Feldstein (2000).

What it seems more relevant is that the characterization of some non-linear aspects of atmospheric variability, related to features of the data distribution of the associated RPC time series are dependent upon the time averaging applied and in some cases on the reanalysis used. It deserves especial mention that the use of parametric and non-parametric parameters of the distributions are not exactly interchangeable and that non-parametric measures captures better some characteristics of the distributions. These former results agree with those of Teng et al. (2004) who, in the framework of climate regimes, pointed forward that perhaps the most straightforward method to assess the sensitivity of these structures to averaging is the systematic study of the non-gaussian structure of the data.

6. Acknowledgements

The authors gratefully acknowledge the scientists involved in producing the ERA-40 and NCEP Reanalyses.

7. Bibliography

Barnston, AG and RE Livezey (1987). Classification, seasonality and persistence of low- frequency atmospheric circulation patterns. *Mon. Wea. Rev.*, 115, 1083-1126.

Branstator, G (2002). Circumglobal teleconnections, the jetstream waveguide, and the North Atlantic Oscillation. *J. Climate*, 15, 1983-2010.

Bell, GD and MS Halpert (1995). Atlas of intraseasonal and interannual variability, 1986-1993, NOAA Atlas No 12, Climate Prediction Center, NOAA/NWS/NMC, Washington DC.

Blackmon, ML et al. (1984). *Journal of Atmospheric Sciences*, vol 41, Issue 6, pp 961-980.

Bloomfield, P (1976). Fourier Analysis of Time Series: An Introduction. Wiley, NewYork.

Doblas-Reyes, FJ and M Déqué (1998). A flexible bandpass filtering procedure applied to midlatitude intraseasonal variability. *Mon. Weather Rev.*, 126, 3326-3335.

Feldstein, SB (2000). The timescale, power spectra and climate noise properties of teleconnection patterns. *J. Climate*, 13, 4430-4440.

Franzke, C et al. (2004). Is the North Atlantic Oscillation a breaking wave? *J. Atmos. Sci.*, 61, 145-160.

García Pérez, A (2002). Estadística aplicada: conceptos básicos. Universidad Nacional de Educación a Distancia, 405 pp.

Hannachi, A et al. (2003). Probability based methods for quantifying nonlinerity in the ENSO. *Climate Dynamics*, 20, 241-256.

Hannachi, A (2004). A Primer for EOF Analysis of Climate Data Department of Meteorology, University of Reading, Reading RG6 6BB, UK, pp 33.

Jolliffe, IT and D Stephenson (2003). Forecast Verification. Willey, New York, 240 pp.

Kalnay, E et al. (1996). The NCEP/NCAR 40 year reanalysis project. *Bull. Amer. Meteor. Soc.* 77, 437-471.

Kushnir, Y and JM Wallace (1989). Low-frequency variability in the Northern Hemisphere winter: Geographical distribution, structure and time-scale dependence. *J. Atmos. Sci.*, 46, 3122-3142.

Metz, W (1991). Optimal relationship of large-scale low patterns and the barotropic feedback due to high-frequency eddies. *J. Atmos. Sci.*, 48, 1141-1159.

Monahan, AH (2000). Nonlinear principal component analysis by neural networks: Theory and application to the Lorenz system. *Journal of Climate*, 13(4): p 821-835.

Panagiotopoulos, F et al. (2002). A Review of Northern Hemisphere Winter-time Teleconnection Patterns. *Journal de Physique IV France*, 12: Pr 10-27 - Pr 10-47.

Quadrelli, R and JM Wallace (2004). A simplified linear framework for interpreting patterns of Northern Hemisphere wintertime climate variability, *Journal of Climate*, 17, 19, 3728-3744.

Richman, MB (1986). Rotation of principal components. *J. Climatol.*, 6, 293-335.

Rodionov, S and R Assel (2001). A new look to the Pacific/North Americen index. *Geophys. Res. Lett.*, 28, 1519-1522.

Silverman, BW (1986). Density Estimation for Statistics and Data Analysis. Chapman and Hall, London, 175 pp.

Teng, Q, AH Monahan and JC Fyfe (2004). Effects of Time Averaging on Climate Regimes. *Geophys. Res. Lett.*, 31, 1-4.

Thompson, DWJ and JM Wallace (2001). Regional Climate Impacts of the Northern Hemisphere Annular Mode. *Science*, 293, 85-89.

Uppala, S et Co-authors (2005). ECMWF reanalysis 1957-2001, ERA-40 Project Series 3 Workshop on Reanalysis. ECMWF, Reading, UK, 62 pp.

Von Storch, H and FW Zwiers (1999). Statistical Analysis in Climate research. Cambridge University Press, 510 pp.

Wallace, JM and DS Gutzler (1981). Teleconnections in the geopotential height field during the Northern Hemisphere winter. *Mon. Wea. Rev.*, 109, 784-812.

Wilks, DS (1995). Statistical Methods in the Atmospheric Sciences, Academic Press, 467 pp.

8. List of tables

Table 1:
Fraction of total variance (%) of the ERA-40 teleconnection patterns.

	Daily data (C1)	10-day low-pass filtered data (C2)	Monthly data (C3)
NAO	5.2	6.5	9.5
SCA	5.1	6.5	7.1
PNA	5.2	6.6	11.0
WP	4.8	5.8	7.4

Table 2:
Spatial correlation coefficients for the ERA-40 teleconnection patterns between different timescales.

	Daily data vs 10-day low-pass filtered data	Dayly data vs monthly data	10-day low-pass data vs monthly data
NAO	0.97	0.91	0.95
SCA	0.99	0.94	0.95
PNA	0.98	0.90	0.93
WP	0.99	0.95	0.95

Table 3:
ERA-40 Skewness (b_1) coefficient.
The coefficients in bold are significant with a 95% confidence.

	Daily data (C1)	10-day low-pass filtered data (C2)	Monthly data (C3)
NAO	-0.13	-0.27	-0.12
SCA	0.11	0.14	0.33
PNA	-0.43	-0.45	-0.08
WP	-0.49	-0.48	-0.44

Table 4:
ERA-40 Kurtosis (b_2- 3) coefficient.
The coefficients in bold are significant with a 95% confidence.

	Daily data (C1)	10-day low-pass filtered data (C2)	Monthly data (C3)
NAO	-0.31	-0.27	0.09
SCA	-0.16	-0.15	-0.37
PNA	-0.12	-0.11	-0.64
WP	0.23	0.09	-0.05

Table 5a:
Median (MED), interquantile-range (IQR) and Yule-Kendall skewness (YKI) for ERA-40.

	Daily data (C1)			10-day low-pass filtered data (C2)			Monthly data (C3)		
	MED	**IQR**	**YKI**	**MED**	**IQR**	**YKI**	**MED**	**IQR**	**YKI**
NAO	0.055	1.394	-0.070	0.078	1.407	-0.077	-0.027	1.195	0.107
SCA	-0.037	1.375	0.053	-0.038	1.447	0.046	-0.113	1.324	0.109
PNA	0.088	1.407	-0.061	0.092	1.407	-0.075	0.015	1.432	-0.049
WP	0.092	1.298	-0.040	0.113	1.298	-0.094	0.155	1.164	-0.206

Table 5b:
Median (MED), Interquantile-Range (IQR) and Yule-Kendall Index (YKI) for NCEP.

	Daily data (C1)			10-day low-pass filtered data (C2)			Monthly data (C3)		
	MED	**IQR**	**YKI**	**MED**	**IQR**	**YKI**	**MED**	**IQR**	**YKI**
NAO	0.050	1.385	-0.063	0.071	1.413	-0.075	-0.028	1.277	0.153
SCA	-0.040	1.379	0.058	-0.037	1.393	0.040	-0.045	1.356	-0.018
PNA	0.076	1.416	-0.039	0.096	1.402	-0.089	0.056	1.410	-0.062
WP	0.101	1.285	-0.044	0.119	1.295	-0.101	0.145	1.222	-0.203

9. Figures

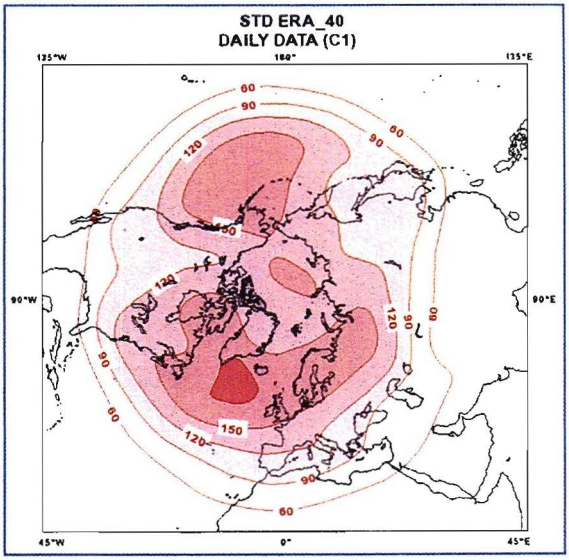

Figure 1. *Standard deviation of ERA-40 daily data. Contour interval: 30 m*

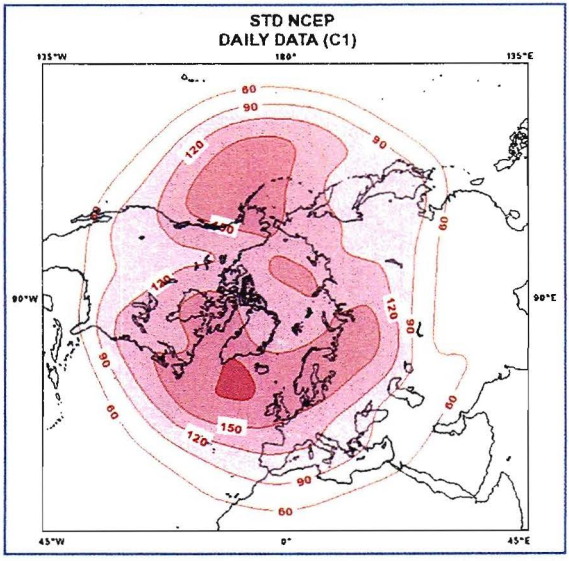

Fig. 1 (cont.). *Standard deviation of NCEP daily data*

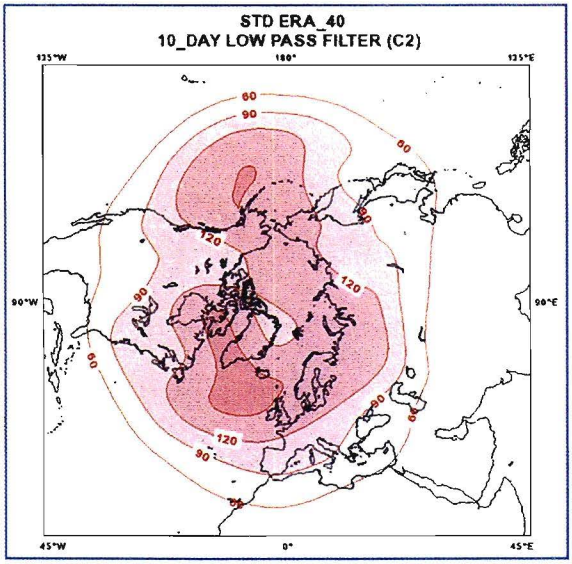

Fig. 1 (cont.). *Standard deviation of ERA-40 10-day low-pass filtered data*

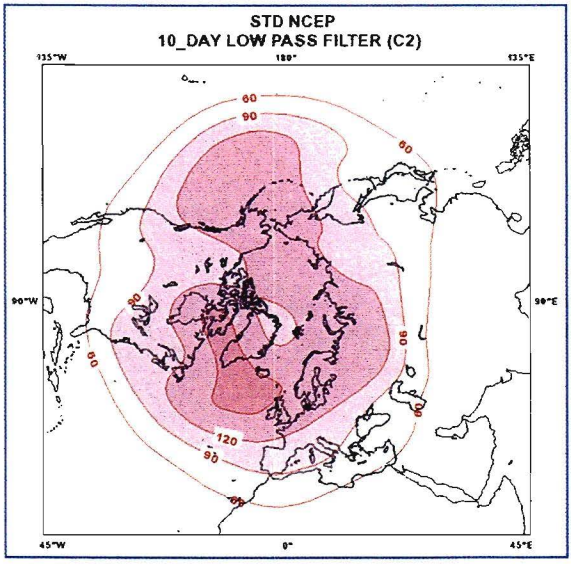

Fig. 1 (cont.). *Standard deviation of NCEP 10-day low-pass filtered data*

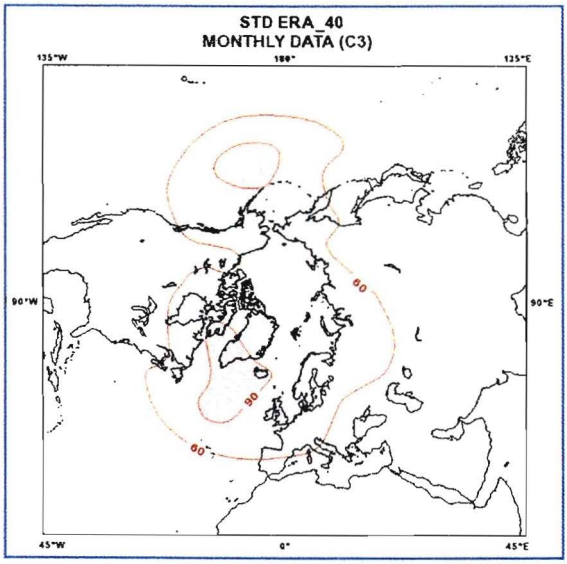

Fig. 1 (cont.). *Standard deviation of ERA-40 monthly data*

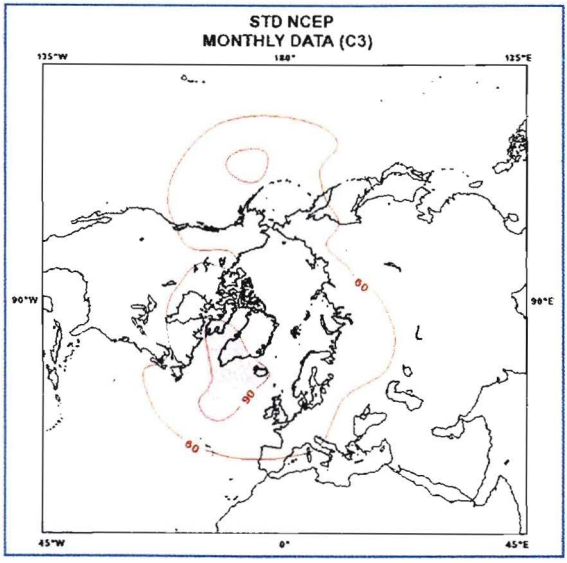

Fig. 1 (cont.). *Standard deviation of NCEP monthly data*

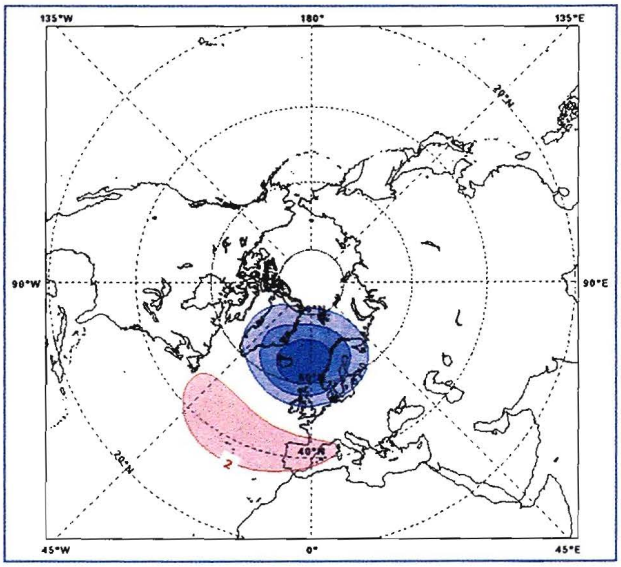

Figure 2. *ERA-40 NAO pattern of daily data. Contour interval is 0.4 hPa*

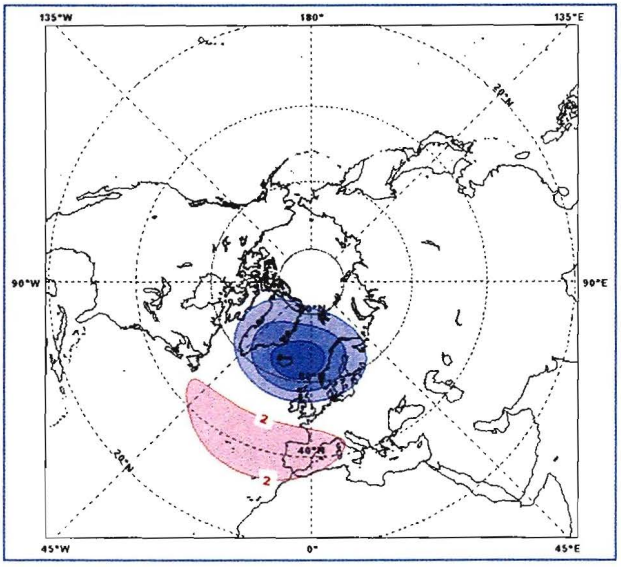

Fig. 2 (cont.). *ERA-40 NAO pattern of 10-day low-pass filtered data*

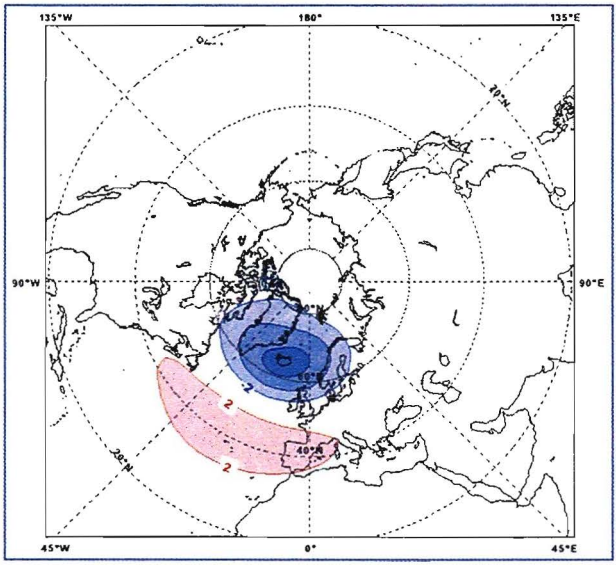

Fig. 2 (cont.). *ERA-40 NAO pattern of monthly data*

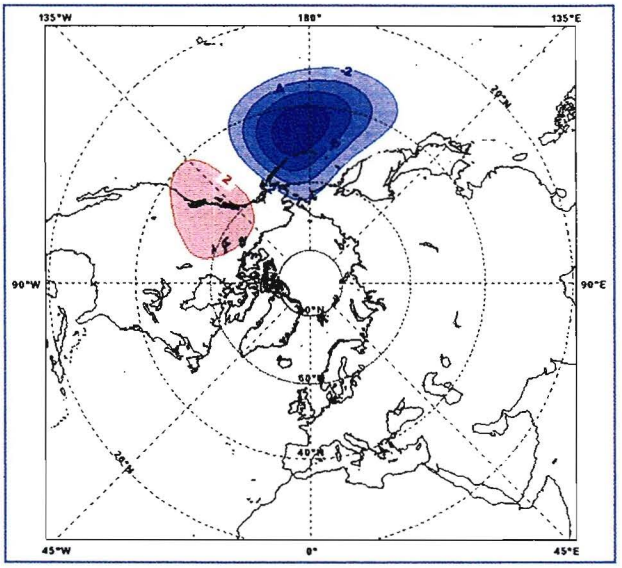

Figure 3. *ERA-40 PNA pattern of daily data*

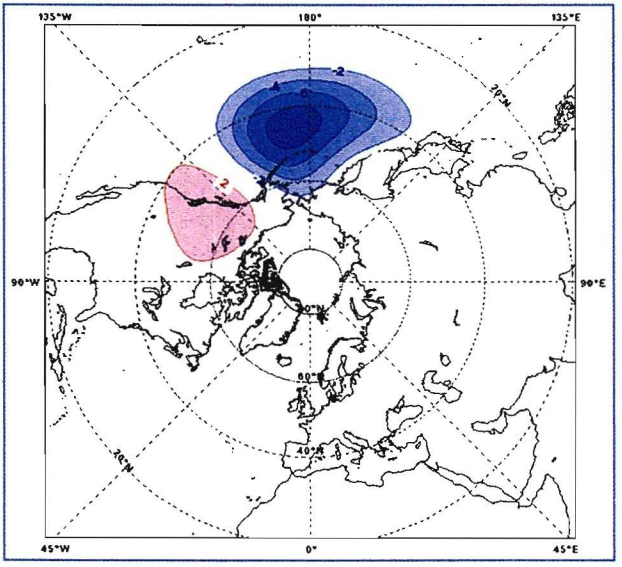

Fig. 3 (cont.). *ERA-40 PNA pattern of 10-day low-pass filtered data*

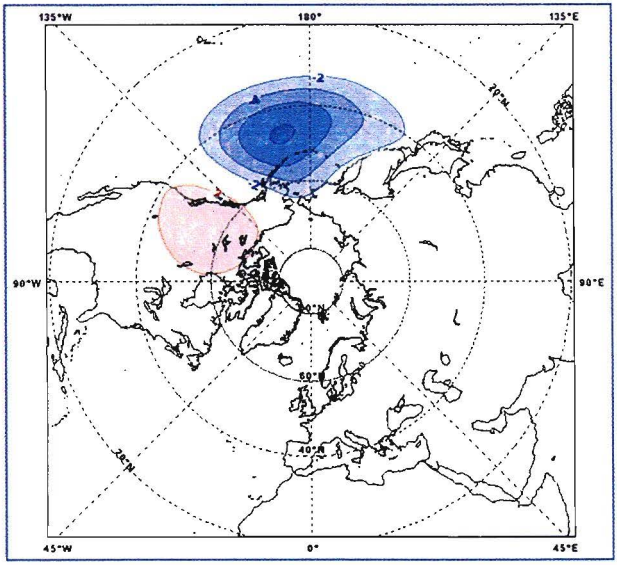

Fig. 3 (cont.). *ERA-40 PNA pattern of monthly data*

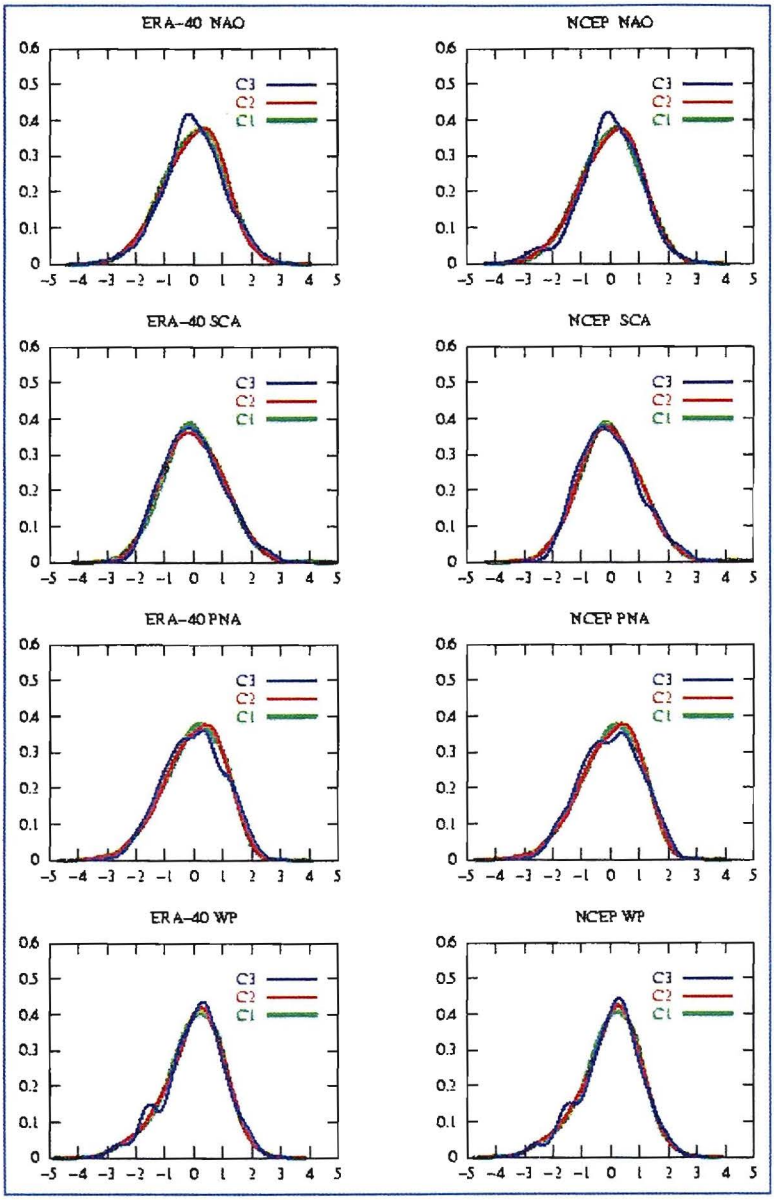

Figure 4. PDFs of NAO, SCA, PNA and WP for ERA-40 (left) and for NCEP (right)

ISBN: 84-8320-360-X

9 788483 201930

3,00 €
IVA incluido

MINISTERIO
DE MEDIO AMBIENTE

SECRETARÍA
GENERAL TÉCNICA

CENTRO DE PUBLICACIONES

AE